



TITLE:

# Some fluidized landslides triggered by the 2011 Tohoku Earthquake (Mw 9.0), Japan

AUTHOR(S):

Wang, Gonghui; Suemine, Akira; Zhang, Fanyu;  
Hata, Yoshiya; Fukuoka, Hiroshi; Kamai, Toshitaka

---

CITATION:

Wang, Gonghui ...[et al]. Some fluidized landslides triggered by the 2011 Tohoku Earthquake (Mw 9.0), Japan. *Geomorphology* 2014, 208: 11-21

ISSUE DATE:

2014-03-01

URL:

<http://hdl.handle.net/2433/183219>

RIGHT:

© 2013 Elsevier B.V.; This is not the published version. Please cite only the published version.; この論文は出版社版ではありません。引用の際には出版社版をご確認ご利用ください。

## Some fluidized landslides triggered by the 2011 Tohoku Earthquake (M9.0), Japan

Gonghui Wang<sup>a\*</sup>, Akira Suemine<sup>a</sup>, Fanyu Zhang<sup>b</sup>, Yoshiya Hata<sup>c</sup>, Hiroshi Fukuoka<sup>a</sup>, Toshitaka Kamai<sup>a</sup>

<sup>a</sup> *Research Center on Landslides, Disaster Prevention Research Institute, Kyoto University, Gokasho, Uji, Kyoto, 611-0011, Japan*

<sup>b</sup> Department of Geological Engineering, Lanzhou University, Tianshui Road, 222, Lanzhou, 730000, P.R. China

<sup>c</sup> Graduate School of Engineering, Osaka University, Yamada Oka 2-1, Suida, 565-0871, Osaka, Japan

\* Corresponding author. Tel: +81-774-384115; Fax: +81-774-384300

E-mail address: wanggh@landslide.dpri.kyoto-u.ac.jp (G. Wang)

## 1 Abstract

2 The 2011 Tohoku Earthquake off the Pacific coast of Japan generated a large tsunami and many landslides,  
3 resulting in a great number of casualties. Although almost all casualties resulted from the tsunami, some  
4 long-travel, fluidized small-scale landslides also killed 13 people. After the earthquake, we surveyed seven of  
5 these catastrophic landslides triggered by the earthquake. We found that most of them have nearly identical  
6 geological features, with slopes consisting of pyroclastic deposits formed at different times, and with a palaeosol  
7 layer that outcropped in most cases after the landslide. Above the palaeosol there are layers of pumice and  
8 scoria. The palaeosol had a natural moisture content of ~160%, and the pumice and scoria a moisture content of  
9 ~145%. From field observations we concluded that the sliding surface originated in the very upper part of  
10 palaeosol, and liquefaction occurred in both layers, resulting in the fluidization of displaced landslides. To  
11 examine the trigger and movement mechanism of these landslides, we monitored the ground motion of one  
12 landslide area during the many aftershocks, and compared the results with records obtained by a national seismic  
13 station nearby. We inferred that strong seismic motion occurred in the landslide area during the main shock. We  
14 sampled the palaeosol and pyroclastic deposits, and performed undrained static/cyclic shear tests on the materials  
15 both in a saturated state and at natural moisture content. The results indicate that high pore-water pressure  
16 generated, resulting in decreased shear strength even in samples with the natural moisture content. The shear  
17 strength of the palaeosol lowered to a very small value with continuous increase of shear rate, enabling the high  
18 mobility of the displaced landslide materials.

19  
20 Keywords: Earthquake-induced landslide; the 2011 Tohoku earthquake; Pore-water pressure; Partially saturated  
21 soils; Strong ground motion

## 1. Introduction

An earthquake of magnitude 9.0 ( $M_w$ ) occurred at 14:46 JST on 11 March 2011, off the Pacific coast of the Tohoku Region, adjacent to the northeastern part of the Japanese mainland (Fig. 1). This "2011 Tohoku Earthquake" is the strongest one known to have hit Japan. The earthquake triggered an extremely powerful tsunami, causing many casualties (15,883 confirmed deaths, 2,656 missing, and 6,145 injured as of 9 August 2013, according to the Japanese National Police Agency) and severe destruction of infrastructure in the Tohoku Region.

Many landslides were triggered by this earthquake in the wider Tohoku Region, with some concentrated in the southern part of Fukushima Prefecture, in hilly residential areas of Miyagi and Fukushima Prefectures, and on island areas of the Matsushima coast. Although the landslides were small for the magnitude of the earthquake (compared to those landslides triggered by previous  $M_j = 7-8$  earthquakes in the same area; Doshida and Uchiyama, 2012), many showed very high mobility, with features typical of flowslide (fluid-like motion of granular material; Bishop, 1973). The fluidized, rapid, long-travel movement of these landslides attracted attention of geotechnical researchers and engineering geologists, because the landslides were scattered in different areas, experienced little preceding precipitation, and displayed no evidence of occurrence beneath the groundwater table. Understanding the initiation and movement mechanisms of these landslides is of great importance to the mitigation of future coseismic geohazards. After the earthquake, we undertook a reconnaissance field examination of the landslides, and investigated seven of them in detail. Here we describe two landslides that occurred in the south part of Fukushima Prefecture and one in Tochigi Prefecture, and discuss their possible initiation and movement mechanisms. By monitoring a landslide area during frequent aftershocks, we could estimate the seismic response of the landslide area during the main shock which triggered the slope instability. Through geotechnical tests on the shear behavior of the landslide materials for different moisture contents, the post-failure behaviour of the landslide was inferred.



## 2. Study area

There were many landslides that occurred in southern Fukushima Prefecture and northern Tochigi Prefecture. As samples of catastrophic landslides, we present data from two landslides (Hanokidaira and Shirasawa) from Shirakawa City, and one occurring in the Oshino area (Fig. 1). Fig. 2 presents a geologic map of the study area, which was based on the 1:200,000 Seamless Digital Geological Map of Japan (Geological Survey of Japan, 2003). This area mainly consists of Mesozoic granite, Paleozoic and Mesozoic sedimentary/ metamorphic rocks, Neogene volcanic rocks and sedimentary rocks, and Quaternary fluvial deposits. All these three landslides occurred in Pleistocene tephra and highly weathered welded tuff in hilly areas in the eastern part of the Ōu Mountains. In the strata of the landslide areas, 12 layers of tephra resulting from eruptions of Nasu Volcano at different times are recognized (Suzuki, 1992). In the following sections, geological details of each landslide are introduced.

Fig. 3 shows the topography of the areas with the Hanokidaira (Fig. 3a), Shirasawa (Fig. 3b), and Oshino (Fig. 3c) landslides. Fig.3a was based on the urban plan map (1/2500) of Shirakawa City, Fukushima Prefecture, while Figs. 3b and 3c were taken from the digital maps of the Geospatial Information Authority of Japan, because the urban plan maps in the scale of 1/2500 for these landslide areas are not available. The prefailure slope of each landslide was steep, and recent fluvial erosion cut and steepened the slope toe (Chigira, 2011).

## 3. Methods

We measured their after-event topography using a laser rangefinder (TruPulse360<sup>o</sup>B with a resolution of 0.1 m). We also used images from Google Earth to examine the topography of these landslides both before and after the earthquake.

We used a portable seismometer (Character frequency: 1.9–2.1 Hz; Measurable amplitude of vibration:  $\pm 2$  mm; Sensitivity coefficient:  $0.8 \text{ v kine}^{-1}$ ) to monitor earthquake aftershocks at the Hanokidaira landslide. This seismometer has been developed for dense seismic observation, and has an extremely low power consumption (<

0.08 W). It records seismic movement continuously for six months using eight dry-cell batteries, at a sampling rate of 250 Hz archiving one file per minute. We monitored aftershocks at the site during April 11–29, 2011 and obtained many records.

We employed a series of intelligent ring-shear apparatuses developed at the Disaster Prevention Research Institute, Kyoto University (Sassa et al., 2004), to examine the static and cyclic shear behaviors of samples that were taken from near the sliding surfaces of the landslides. These samples were fully saturated or kept at their natural moisture content during the shear tests, and were sheared under undrained conditions.

## 4. Results

### 4.1 Features of fluidized landslides

#### 4.1.1 Hanokidaira landslide

The Hanokidaira landslide (Fig. 4a) originated on a southeast-facing slope of a hill located about 1 km north of JR Shirakawa Station in Shirakawa City. Thirteen people were killed and 10 houses were destroyed by the debris of the landslide. A small portion of the displaced material spilled into a golf driving range, forming a thin deposit.

Stratigraphically from bottom to top, the slope consists of a basal deeply weathered welded tuff, a palaeosol, weathered pumice and scoria partly with palaeosols, and forest soil. The bedded texture is approximately parallel to the slope surface. The primary palaeosol, which overlies the welded tuff, outcropped, and had striations on its surface (Fig. 4b). We dug into the deposits on the golf driving range and found that grass was flattened and buried by the displaced materials, but not cut or displaced from its original place (Fig. 4c). Above the grass was a displaced ~10 cm thick palaeosol layer overlain by loose pumice. Many trees had stood almost vertically while being transported. There were muddy striae on the left flank of the landslide (Fig. 4d) and also splashes of mud on the high position above the sliding surface (Fig. 4e), indicating that the displaced mass experienced slide at first and then liquefaction, and the liquefied materials (mud) were splashed

during downslope movement. Therefore, the movement of this landslide can be classified as earth *slide-flow*, according to Cruden and Varnes (1996).

Using the above-mentioned laser rangefinder, we surveyed the landslide area to prepare a longitudinal section (Fig. 4f). The main part of the displaced materials spread into a residential area at the foot of the hill, exhibiting substantial fluid-like flow. The apparent mobilized friction angle of the slide was about  $9.6^\circ$ , measured from point I to I' in Fig. 4a. According to the measured topography, we estimated that the volume of the displaced material was about  $100,000 \text{ m}^3$ , with a horizontal travel distance of about 290 m and a total relief of about 50 m.

No standing ground water or groundwater seepage was found in the landslide source area. However, local residents told us that there was a continuous spring at the toe part of the slope. Therefore, we inferred that standing ground water existed in the slope before the occurrence of the landslide. Due to stabilization countermeasures, the debris on the lower part of the slope, near point T in Fig. 4a, has been removed and the slope continues to yield water from small springs (observation in July 2012).

At the Hanokidaira landslide source area, tephra layers exposed during excavation for stabilization. The existence of palaeo-valley had been identified (Fig. 4g). The upper surface of the welded tuff (and the palaeosol) indicates a substantially dissected hilly area with a palaeo-valley aligned approximately east–west and sloping to the east (PV-M in Fig. 4g). The palaeo-valley had a tributary (side valley) sloping up towards the present highest point in the local landscape (PV-T in Fig. 4g). The most prominent palaeosol in the sequence is developed on this hilly palaeo-surface, which was subsequently mantled and largely buried by thick layers of air-fall volcanic ash. Through erosional reworking of the tephra during the long interval during which all of the layers were deposited, the thickness of the ash pile along the axis of the palaeo-valley has become greater than that on the flanks of the palaeo-valley. The landslide has substantially cleaned out the tephra down to the palaeosol developed on the weathered welded tuff.

#### 4.1.2. Shirasawa landslide

The Shirasawa landslide (Fig. 5) is located approximately 4 km northeast of the Hanokidaira landslide. It originated from a gully head. Like the Hanokidaira landslide, the soil layers in the source area, from the bottom to the ground surface, are a palaeosol, pumice, and weathered volcanic ash with pumice. The bedded texture approximately parallels to the slope surface. The displaced materials slid from the source area above the palaeosol (Fig. 5b), and the left flank was also imprinted by muddy striae and splashes of mud on a high position above the sliding surface (Fig. 5c). Therefore, the movement can be classified as earth *slide-flow* like the Hanokidaira landslide. The landslide began on a 13° slope, slid onto a slope of 46°, then turned south and travelled 230 m along the valley. The total flow length of the slide was 331 m, with a relief of 70 m, giving an apparent mobilized friction angle of 11.9°. The source area was 95 m long, 30 m wide and 3 m thick on average, giving a landslide volume of about 9000 m<sup>3</sup>. This landslide occurred in a non-residential area and no casualties or injuries were reported.

#### 4.1.3. Oshino landslide

The Oshino landslide (Fig. 6a) is located 45 km south of Shirakawa City. The landslide originated on a northeast- to north-facing slope, below which are terraced paddy fields. The source area is 45 m long, 55 m wide and 4 m thick on average; therefore the landslide volume was approximately 10,000 m<sup>3</sup>. The displaced materials traveled about 100 m across a rice paddy, and then descended a 10 m steep step and continued for further 65 m across a lower rice paddy (Fig. 6d). The apparent mobilized friction angle of this landslide was 9.5°. The deposits had a thickness of about 3 m in both paddies. Many trees were standing vertically on the landslide toe. We dug a pit at the toe and found that the rice paddy soil had been barely disturbed.

The soil layers of the source area were a palaeosol, weathered volcanic ash, and pumice respectively from the base of the sliding surface to the top. Fig. 6b presents the outcropped sliding surface with palaeosol

underlain. The bedded texture approximately parallels to the slope surface. On the left flank, muddy striae and splashes of mud on the high position above the sliding surface were also observed (Fig. 6c), indicating that this landslide can be classified as earth *slide-flow* according to the movement of displaced mass. A witness reported that the sliding occurred and stopped in some seconds during the strong seismic motion.

#### 4.2. Seismic motion

Japan has a dense network of seismic stations including two permanent strong-motion stations in Shirakawa City: a Kyoshin Network (K-NET Shirakawa) station of the National Research Institute for Earth Science and Disaster Prevention (NIED), Japan, and a station operated by the Japan Meteorology Agency (JMA Shirakawa-shi Kakunai station). The seismic waves recorded by these two stations during the main shock are presented in Fig. 7a-f, respectively. At both stations, the vertical component of motion was the smallest, and N–S component the greatest. Nevertheless, the peak values were different. The K-NET station had a peak acceleration of 1295.2 gal, while the JMA station recorded a maximum of 371.5gal, about one-third of the former. The K-NET station is about 2.8 km southwest of the Hanokidaira landslide, while the JMA station is about 800 m south. Therefore, the landslide may have experienced a similar level of a seismic response as that at the JMA station during the main shock. However, seismic responses of a site depend greatly on the local characteristics of soil/rock layers and topography. To better understand the seismic motion of the Hanokidaira area, we installed a seismometer close to the top of the landslide area on April 11, 2011 to record aftershocks and estimated the seismic response during the main shock (Fig. 7g-i) by means of the site-effect substitution method (Hata et al., 2011, 2012). The estimated seismic wave had a peak acceleration of about 907 gal in an N–S direction and 778 gal in an E–W direction, about 2.4 and 2.3 times greater than the records from the JMA station respectively. Although the estimated vertical acceleration had a smaller peak value of 463 gal, this value is about 3.4 times greater than that recorded at the JMA station, indicating that the Hanokidaira landslide area had a stronger site

effect on the vertical motion. From Fig. 7g-i, we infer that the peak seismic motion on the slope at Hanokidaira was greater than 1 g, and triggered the failure during the main shock.

### 4.3. Geotechnical aspect

#### 4.3.1. Setup of shear test

Field surveys revealed that all these landslides had a palaeosol as their basal layer, and all the materials above this layer had been displaced. This suggests that the boundary between the palaeosol layer and the overlying pumice layer played a key role in the initiation and movement of the landslides, and the shear failure formed a sliding surface in both soil layers. Although our field surveys failed to find standing water, i.e., the soil layers might not have been in a fully saturated state, we found that the field moisture content of these soil layers was very high. Also the landslides were all triggered on slopes with small valleys below where ground water tends to converge. We infer that the soil layers near the sliding surface had a very high moisture content or been nearly saturated, and hence liquefaction led to the high mobility of these landslides.

In 2011, disturbed samples of more than 40 kg were taken from the palaeosol (S1) and pumice with scoria (S2) in the source area of each landslide for geotechnical tests. In July 2012, we also took intact samples from the palaeosol layer of the Hanokidaira landslide exposed during stabilization work (S1' in Fig. 4). Two blocks (about 40×40×30 cm for each) were taken and transported in plastic bags to keep moisture content.

At first, we performed direct shear box tests on intact and remolded samples of S1 taken from the Hanokidaira landslide to examine the shear strength of S1 in intact state and also to examine the possible difference between the intact and remolded samples. We also performed undrained shear tests on the remolded samples of S1 and S2 taken from all these landslides at natural moisture content or fully saturated state, and found that they all can be fully liquefied. In the following, we present the results from tests on the samples taken from the Hanokidaira landslide as an example. S1 from the Hanokidaira landslide had a specific gravity of

approximately  $2.70 \text{ g cm}^{-3}$ , dry density of  $0.48\text{--}0.66 \text{ g cm}^{-3}$ , natural moisture content of 94–160% and void ratio of 3.10–4.18, while sample S2 had a specific gravity of 2.68  $\text{g cm}^{-3}$ , dry density of  $0.51\text{--}0.64 \text{ g cm}^{-3}$ , natural moisture content of 94–151%, and void ratio of 3.25–4.25. The intact blocks of S1 had a natural moisture content of 114% and dry density of  $0.636 \text{ g cm}^{-3}$ .

Because the tests were carried out to examine the shear behavior of the soil in the source area, test conditions were designed to represent a soil element on the sliding surface overlain by an 8 m thick soil (measured vertically) for the Hanokidaira landslide. The normal and shear stresses on the sliding surface were calculated using a slope angle of  $16^\circ$  (Fig. 4f), and a unit weight of  $11.4 \text{ kN m}^{-3}$ , which was calculated from the measured in situ density of the sample, assuming that no groundwater table existed in the slide. Thus, the estimated normal stress ( $\sigma_i$ ) was 84 kPa and shear stress ( $\tau_i$ ) was 24 kPa.

We performed direct shear box tests on the intact or remolded sample of S1 under consolidated drained conditions following the standard of ASTM D3080. The shear box, assembled with the top and bottom halves of the box screwed, has a size of  $10 \times 10 \times 10 \text{ cm}$ . The remolded samples were prepared to be approximately the same initial dry density as the intact one. We sheared the sample at natural moisture content and also at fully saturated state. For saturated tests, we put the shear box with sample into distilled water for 4 days to ensure full saturation.

We performed undrained ring shear tests on saturated samples following these steps: (1) putting remodeled S1, directly taken from the intact blocks in natural water content without any dry process, or air dried S2 into the shear box; (2) saturating the samples using  $\text{CO}_2$  and de-aired water; (3) normally consolidating the sample under a given stress state; (4) undrained shearing the sample by applying cyclic loadings or increasing only shear stress (static shearing). For tests on samples with the natural moisture content, we put the remolded natural samples into the shear box and then went through steps (3) and (4). More detailed procedures for performing undrained shear tests in a ring shear apparatus are described by Sassa et al (2003).

We also performed undrained shear tests on fully saturated air-dried or oven-dried samples of S1 to examine the possible effect of drying process on its undrained shear behavior. As pointed out by Chigira et al (2012), the dominant clay mineral in the palaeosol of the studied landslides is halloysite, which is normally formed by hydrothermal alteration of volcanic rocks (Kerr, 1952); while air or oven drying would result in the dehydration of interlayer water of halloysite (Wesley, 1973, 1977; Okada and Ossaka, 1983). Nevertheless, detailed examination on the possible effects of drying process on palaeosol properties is beyond the focus of this study; here we only present the results of tests on those samples with natural moisture contents.

#### 4.3.2. Results of direct shear box tests on samples S1

We performed direct shear box tests under differing normal stress levels (84, 64 and 41 kPa, respectively). The intact samples were kept at natural moisture contents or fully saturated, while the remolded samples were kept at their natural moisture contents. The representative failure envelopes from these tests are shown in Fig. 8. The intact sample at natural moisture content presented an angle of shearing resistance of  $\phi' = 27^\circ$  with an apparent cohesion,  $c$ , of 22 kPa (Fig. 8). These strength parameters varied greatly when the sample was remolded, showing  $\phi' = 14^\circ$  and  $c = 26$  kPa. Fully saturated intact sample behaved slight change in the strength parameters, showing  $\phi' = 26^\circ$  and  $c = 19$  kPa, probably because the natural moisture content was originally very high (the saturation degree was 94.3%).

Consolidated drained triaxial compression tests were also conducted on the intact and remolded samples of S2 taken from the location shown in Fig. 4, and the results showed that saturated intact S2 has  $\phi' = 33.0^\circ$  and  $c = 37.4$ , while the saturated remolded S2 has  $\phi' = 34.2^\circ$  and  $c = 2.7$  (K. Sasahara, personal communication, January 12, 2012). The failure envelopes for intact and remolded samples of S2 were compared to these of S1 in Fig. 8. Intact S2 has a greater shear strength than intact S1 at any given normal stress.



#### 4.3.3. Results of cyclic shearing at natural moisture contents

Undrained cyclic shear tests were conducted on both samples at natural moisture contents (114% and 140% for S1 and S2, respectively). After being placed in the shear box and normally consolidated, the samples were subjected to a cyclic shear stress, with an amplitude of 24 kPa (i.e., 24 kPa cyclic load superimposed onto the 24 kPa gravitational shear load) and a frequency of 0.5 Hz under undrained conditions. We used this low-frequency for better monitoring the response of pore-water pressure that might be generated during the shearing. Fig. 9 presents the results as time series data for both samples. In these tests, normal stress was kept constant. However, the cyclic shear stress was not faithfully applied by the control system, probably because this ring shear apparatus was designed for high stress level (maximal normal stress: 2 MPa), and the cyclic shear stress of 24 kPa is relatively too small. Nevertheless, in both tests, shear failure was triggered due to the introduction of cyclic shear loading, and continued even after the cyclic shear loading ceased. With continuing cyclic shearing, the shear resistance became smaller than the initial shear stress. This enabled continuing shear failure and shear resistance lowered further to approximately zero.

The monitored pore-water pressure was small, likely due to the air left inside the samples and also inside the pore-water pressure measuring system. The highly compressible air would cause a delayed reaction to the change in pore-water pressure. The low permeability of the sample (clayey soil) may also delay the response of the pore-water pressure monitoring system, because the excess pore water pressure was generated within the shear zone, while the pore-water pressure measuring system was installed near but outside of the shear zone (Wang et al, 2007). Disturbed sample S2 has a permeability of approximate  $2.9 \times 10^{-2} \text{ cm s}^{-1}$  at a dry density of about  $0.51 \text{ g cm}^{-3}$ , while sample S1 has a permeability of about  $1.3 \times 10^{-5} \text{ cm s}^{-1}$  at a dry density of about  $0.64 \text{ g cm}^{-3}$ , smaller than that of S2. This may be the reason why the monitored excess pore water pressure in Fig. 9a was smaller than that in Fig. 9b. However, we inferred that the excess pore-water pressure built up within the shear zone had reached to a value approximately equal to the total normal stress, such that the shear resistance lowered approximately to zero after 40 seconds in both tests.

Although additional shear stress of about 24 kPa had been applied to the initial shear stress once (Fig. 9a), the applied cyclic shear stress was smaller than 24 kPa in general, resulting in changes in the number of cycles necessary for the initiation of shear failure, but has no effect on the post failure shear behavior (Wang, 2000). Therefore, considering the strong motion and long duration of the main shock of the earthquake and the inferred degree of saturation, we concluded that liquefaction occurred within the soil layers near the sliding surface.

#### 4.3.4. Results of static shearing at natural moisture content

Considering that the side wall of the landslide mass would suffer from static shearing after the landsliding was initiated by the earthquake, we performed static shearing test on sample S2. In the shear box, the sample with a moisture content of 140% was normally consolidated under the normal stress of 84 kPa and shear stress of 24 kPa, and then sheared by increasing shear stress monotonically under undrained condition. Fig. 10 shows an example of the results of this test. With increasing shear stress, excess pore water pressure was built up gradually. After shear failure occurred, shear resistance gradually lowered to a very small value close to zero. Vertical displacement (positive with sample consolidation) also occurred as shearing progressed.

After the test, we opened the drainage system, and found water being expelled from the shear box. Therefore, even though the sample was not fully saturated, the abundant water in the sample allowed generation of high pore-water pressure after shear failure was triggered.

#### 4.3.5. Shear rate dependency of the palaeosol

Once shear failure occurred, we expected that the displaced landslide material might not accelerate at a constant rate due to strength change with shear rate. To examine this effect, we sheared both samples at different shear rates. The samples were first saturated, and consolidated under a total normal stress of about 200 kPa. This normal stress was chosen for a better performance of the control system and comparisons with the results of our previous tests under the same condition. Then the sample was sheared to a residual state using a

shear-speed-controlled method. We performed multistage test, which has been found to produce results similar to the test of individual samples (Bromhead, 1992; Tika et al., 1996; Tiwari and Marui, 2004; Suzuki et al., 2004; Wang et al., 2010). After the measurement of residual shear strength at a given shear rate, we repeatedly changed the shear rate and then measured the residual shear strength at this differing shear rate. Through this method, the residual shear strengths at different shear rates were measured (Fig. 11). We found that the effect of shear rate on the residual shear strength was significant for the palaeosol sample, and that the shear strength of sample S2 was less affected by the shear rate. The residual shear strength was greater than 150 kPa when the shear rate was smaller than  $0.6 \text{ mm s}^{-1}$ , but was smaller than 50 kPa when the shear rate was greater than  $1 \text{ mm s}^{-1}$ . Although the reason for this sharp decrease in shear resistance with shear rate is unclear, it can be concluded that the shear resistance became very small when the displaced material moved faster.

## 5. Discussion

To analyze landside mobility, a parameter of travel angle ( $\varphi_a$ ), sometimes called apparent friction angle, has been widely used (Scheidegger, 1973; Cruden and Varnes, 1996). The parameter is defined as  $\tan\varphi_a = H/L$ , where  $H$  is the landslide height (the difference in elevation between the crown and the tip of the landslide), and  $L$  is the horizontal distance of the landslide from the toe to the head scarp. Small values of  $\varphi_a$  mean high mobility and the value tends to decrease with increasing volume (Scheidegger, 1973; Voight et al., 1983; Legros, 2001; Crosta et al., 2005). In addition, landslides involving volcanic materials usually have higher mobility (Hayashi and Self, 1992; Legros, 2001). Recently studies showed that some small, rapid, fluidized landslides due to rainfall (Wang, 2000) or earthquakes (Crosta et al., 2005) have  $\varphi_a$  of about  $10^\circ$ . The landslides we investigated (Figs. 4 to 6) also had similar  $\varphi_a$  values of  $9.6^\circ$  (Hanokidaira),  $11.9^\circ$  (Shirasawa),  $11.8^\circ$  (Oshino), and  $9.5^\circ$  (Slide I in Fig. 6), showing high mobility, although most of the landslide materials were unsaturated.

Iverson et al. (1997) pointed out that liquefaction plays a key role in the formation of fluidized landslides. In the case of coseismic landslides, the slope instability may result from 1) coseismic force that may make

downslope shear stress greater than shear strength, and (2) buildup of excess pore-water pressure within fully or partially saturated soil layers that may lower the shear strength. In the case of fluidized coseismic landslides, if the excess pore-water pressure increases and the effective normal stress decreases, shear failure may occur, and excess pore-water pressure may further increase with the progress of the failure. As shown in Fig. 8, sample S2 has lower shear resistance than sample S1, indicating that if coseismic force is great enough, the first shear failure occurs within the palaeosol layer. During the subsequent downslope movement of the displaced material, the overlaying soil layer of pumice and scoria experiences further vibration and static shearing, leading to liquefaction. This may be the reason why the deposited landslide materials mainly consist of fluidized pumice with little palaeosol. Therefore, for the risk analysis of fluidized landslides, it is necessary to better understand both the coseismic shear and static shear behaviors of soil layers within a slope.

Numerous tests have been performed on fully saturated sands to examine their liquefaction behavior (c.f., Seed, 1966; Finn, 1981; Ishihara, 1993). However, recent studies reveal that even under unsaturated conditions, sand with a highly compressible soil may liquefy (Kazama et al., 2006; Unno et al, 2006, 2008). The undrained shear tests on samples S1 and S2 (Figs. 9 and 10) indicate that full liquefaction can occur in both samples after shear failure although they are only partially saturated.

The amplification of seismic movement due to slope topography has been recognized (Davis and West, 1973; Ashford et al., 1997; Nishimura and Morii, 1984; Kurita et al., 2003; Buech et al., 2010). Although greater amplification normally occurs on the crest of a slope, the vertical motion of a bedrock-dominated slope is rarely affected by topography (Kurita et al., 2003). Recent studies reveal that the seismic motion especially in the vertical direction is also dependent on the degree of soil saturation resulting in non-linear soil response (Yang and Sato, 2000; Tobita et al, 2010). The estimated seismic motion shown in Fig. 7g-i was based on a practical estimation method of strong ground motion (called “site-effect substitution method”) that was proposed by Hata et al (2011). This method uses the records of aftershocks both at the site of interest and at a nearby permanent strong motion observation station, and the record during the main shock at the observation station. Because this

method takes account of not only the difference of site amplification factors, but also the difference of site phase effects between the site of interest and the observation station, it can estimate time histories of strong ground motion at the site of interest with high accuracy. However, this method does not consider the effect of strong nonlinearity of shallow soft soil, which can greatly change the ground-motion amplification of shallow soil layers (Field, et al., 1997; Beresnev et al., 1998). Therefore, the estimated seismic motion might be representative of the response of engineering bedrock, as considered in the field of earthquake engineering, rather than of shallow soil. The engineering bedrock in earthquake engineering is normally determined by the S-wave velocity ( $V_s$ ) of the bedrock, approximately 300–700 m s<sup>-1</sup>. The seismic motion of surficial soil with smaller  $V_s$  tends to be greater. Further, soil layers in the source area had high moisture content but were not fully saturated. This state could result in a large amplification of vertical motion. We checked the seismic recordings obtained during the aftershocks and found that the vertical motion on the landslide site could be up to about 9 times that recorded by the nearby JMA station, although the estimated vertical motion during the main shock (Fig. 7i) is about 3.4 times that of the JMA records. Although we did not perform further analysis on the possible elastic-plastic earthquake response of the slope, the ground motion of the slope during the main shock may have been much stronger than the estimates in Fig. 7g-i.

In the analysis of coseismic landsliding, the effect of vertical motion on the instability of slopes has been largely ignored. Nevertheless, recent field monitoring and theoretical analysis have revealed that vertical motion also plays an important role in landslide initiation (Yang, 2007). For the studied landslides, strong vertical motion may have contributed to their initiation through two processes: coseismic shear force and compression (or collapse) of unsaturated soil layers, which build up excess pore-water pressure in unsaturated soils during the earthquake. Although the seismic response of a given site to a given earthquake depends on many factors, the direct seismic observation at a landslide site may provide promising data for better understanding the initiation of coseismic landslides.

## 6. Conclusions

During the 2011 Tohoku Earthquake off the Pacific coast of Japan, many landslides were triggered in urban residential regions and on natural slopes, killing more than a dozen people and destroying many homes. These landslides were not very large but characterized by high mobility and a long travel distance. Through field surveys, analyses of seismic motion, and experimental geotechnical examination, their possible initiation and movement mechanisms were examined. The conclusions are as follows.

(1) The landslides in pyroclastic fall deposits showed very high mobility, with the occurrence of liquefaction. Valley incision was distinct at the toe of these landslides, indicating that the upper slope of the landslide source area was less stable state before the earthquake.

(2) Although the epicenter was distant, and the motion recorded by a nearby permanent seismic station was not strong, the seismic motion at the Hanokidaira landslide area was very strong due to local site effects.

(3) For each landslide, the sliding surface was along the boundary between a palaeosol developed on welded tuff and the overlying pyroclastic fall deposits (pumice and scoria). Shear failure might have occurred at first on the palaeosol layer, but liquefaction might have triggered in both the palaeosol layer and the overlaying pumice layer, resulting in the high mobility of displaced landslide materials. These soil layers are highly liquefiable in saturated condition when subjected to cyclic shear loading. High pore-water pressure can also be generated even when the soil layers are not fully saturated.

(4) The shear resistance of the basal palaeosol markedly decreased with increasing shear rate, indicating that in the case of a shear failure within the palaeosol, the shear resistance of the sliding surface might become smaller with an increase of sliding velocity, thus allowing accelerating movement of the displaced landslide materials.

## Acknowledgement

The seismic recordings of the K-NET operated by the National Research Institute for Earth Science and Disaster Prevention (NIED), Japan, and of the Japan Meteorological Agency, were used in this study. This study was supported by two scientific research grants (No. 21403002 and No. 23310125) from the MEXT, Japan. Prof. Masahiro Chigira (Kyoto University), Prof. Katsuo Sasahara (Kochi University), Dr. Marui McSaveney (2012 JSPS Fellow; GNS Science, New Zealand), and Dr. Jun Yang (University of Hong Kong) are thanked for their valuable discussion. Mr. Yao Jiang (Kyoto University) is thanked for their help in the laboratory testing. Valuable English editing by Dr. Eileen McSaveney (GNS Science, New Zealand) is appreciated. Finally, our special thanks go to Mr. William Schulz, Dr. Mauro Soldati, an anonymous reviewer, and Prof. Takashi Oguchi, for their valuable comments that substantially improved this paper.

## References

- Ashford, S.A., Sitar, N., Lysmer, J., Deng, N., 1997. Topographic Effects on the Seismic Response of Steep Slopes. *Bulletin of the Seismological Society of America* 87, 701-709.
- Beresnev, I.A., Field, E.H., Johnson, P.A., Van Den Abeele, K.E.A., 1998. Magnitude of nonlinear sediment response in Los Angeles basin during the 1994 Northridge, California, earthquake. *Bulletin of the Seismological Society of America* 88, 1097-1084.
- Bishop, A.W., 1973. The stability of tips and spoil heaps. *Quarterly Journal of Engineering Geology & Hydrogeology* 6, 335-376.
- Bromhead, E.N., 1992. *Stability of Slopes* (2nd edition). Surrey University Press, London.
- Buech, F., Davies, T., Pettinga, J.R., 2010. The Little Red Hill seismic experimental study: Topographic effects on ground motion at a bedrock-dominated mountain edifice. *Bulletin of the Seismological Society of America* 100, 2219-2229.
- Chigira, M., 2011. Survey results of the landslides (in Fukushima and Tochigi prefectures) and earthquake faults (in Fukushima) occurring during the 2011 off the Pacific coast of Tohoku Earthquake. At: [http://www.dpri.kyoto-u.ac.jp/web\\_j/saigai/tohoku2011/jiban\\_20110426.pdf](http://www.dpri.kyoto-u.ac.jp/web_j/saigai/tohoku2011/jiban_20110426.pdf).
- Chigira, M., Nakasuji A., Fujiwara, S., Sakagami, M., 2012. Catastrophic landslides of pyroclastics induced by the 2011 off the Pacific coast of Tohoku Earthquake. In *Earthquake-induced landslides* (Ugai et al., eds.), *Proceedings of the International Symposium on Earthquake-induced Landslides*, Kiryu, Japan, 2012. pp.139-147.
- Crosta, G.B., Imposimato, S., Roddeman, D., Chiesa, S., Moia, F., 2005. Small fast-moving flow-like landslides in volcanic deposits: The 2001 Las Colinas Landslide (El Salvador). *Engineering Geology* 79, 185-214.
- Cruden D.M., Varnes D.J., 1996. Landslide types and processes. In *Landslides: Investigation and Mitigation* (Turner and Schuster, eds.), National Academy Press, p: 36-71.

- 410 Davis, L.L., West, L.R., 1973. Observed effects of topography on ground motion. *Bulletin of the Seismological Society of*  
411 *America* 63, 283-298.
- 412 Doshida, S., Uchiyama, S., 2012. Features and Distribution of Landslides in the 2011 off the Pacific Coast of Tohoku  
413 Earthquake. *Natural Disaster Research Report of the National Research Institute for Earth Science and Disaster Prevention*  
414 48, 111-120.
- 415 Field, E.H., Johnson, P.A., Beresnev, I.A., Zeng Y., 1997. Nonlinear ground-motion amplification by sediments during the  
416 1994 Northridge earthquake. *Nature* 390, 599-602.
- 417 Finn, W.D.L., 1981. Liquefaction potential development since 1976. *Proceedings of the International Conference on Recent*  
418 *Advances in Geotechnical Earthquake Engineering and Soil Dynamics*, St. Louis, Missouri, 655-681.
- 419 Geological Survey of Japan, 2003. Geological map of Japan at scale 1:200 Million (5<sup>th</sup> version, CD-ROM).
- 420 Hata, Y., Nozu, A., Ichii, K., 2011. A practical method to estimate strong ground motions after an earthquake based on site  
421 amplification and phase characteristics. *Bulletin of the Seismological Society of America* 101, 688-700.
- 422 Hata, Y., Wang, G., Kamai, T., Suemine, A., Nozu, A., 2012. Seismic waveform estimation at the Hanokidaira landslide  
423 induced by the 2011 off the Pacific coast of Tohoku Earthquake based on site effects substitution method. *Journal of*  
424 *Japan Landslide Society* 49(3), 15-24 (in Japanese with English abstract).
- 425 Hayashi, J.N., Self, S., 1992. A comparison of pyroclastic flow and debris avalanche mobility. *Journal of Geophysical*  
426 *Research* 97, 9063– 9071.
- 427 Ishihara, K., 1993. Liquefaction and flow failure during earthquakes. *Géotechnique* 43, 349-451.
- 428 Iverson, R.M., Reid, M.E., LaHusen, R.G., 1997. Debris-flow mobilization from landslides. *Annual Review of Earth and*  
429 *Planetary Sciences* 25, 85–138.
- 430 Kazama, M., Takamura, H., Unno, T., Sento, N., Uzuoka, R., 2006. Liquefaction mechanism of unsaturated volcanic sandy  
431 soils. *JSCE, Journal of Geotechnical Engineering* 62, 546-561 (in Japanese).
- 432 Kerr, P. F., 1952. Formation and occurrence of clay minerals. *Clays and Clay Minerals* 1, 19–32
- 433 Kurita, T., Annaka, T., Takahashi, S., Shimada, M., Suehiro, T., 2003. Effects of irregular topography on strong ground  
434 motion amplification. *Transactions of the 17<sup>th</sup> International Conference on Structural Mechanics in Reactor Technology*  
435 (SMiRT 17), Prague, August 17-22. Paper #K03-1.
- 436 Legros, F., 2001. The mobility of long runout landslides. *Engineering Geology* 63, 301– 331.
- 437 Nishimura, K., Morii, W., 1984. An observed effects of topography on seismic ground motions. *Bulletin of Disaster*  
438 *Prevention Research Institute, Kyoto University*, Vol.34, Part 4, No.310, 203-214.
- 439 Okada, K., Ossaka, J., 1983. Dehydration mechanism of interlayer water of halloysite. *Journal of the Ceramic Association,*  
440 *Japan* 91, 329-334 (in Japanese with English abstract)
- 441 Sassa K., Wang, G., Fukuoka, H., 2003. Performing undrained shear tests on saturated sands in a new intelligent type of ring  
442 shear apparatus. *Geotechnical Testing Journal, ASTM* 26, 257-265.
- 443 Sassa, K., Fukuoka, H., Wang, G., Ishikawa, N., 2004. Undrained dynamic-loading ring-shear apparatus and its application to  
444 landslide dynamics. *Landslides* 1, 1-13.
- 445 Scheidegger, A.E., 1973. On the prediction of the reach and velocity of catastrophic landslides. *Rock Mechanics* 5, 231 - 236.



- 446 Seed, H.B., 1966. Landslides during earthquakes due to soil liquefaction. *Journal of the Soil Mechanics and Foundations*  
447 Division, ASCE 94, 1055-1122.
- 448 Suzuki, T., 1992. Tephrochronological study on Nasu Volcano. *Bulletin of Volcanological Society of Japan (Kazan)* 37,  
449 251-263 (in Japanese with English abstract).
- 450 Suzuki, M., Kobayashi, K., Yamamoto, T., Matsubara, T., Hukuda, J., 2004. Influence of shear rate on residual strength of  
451 clay in ring shear test. *Research Report, School of Engineering, Yamaguchi University* 55(2), 49-62.
- 452 Takeshi, T., 2011. Landslide hazards immediately after the 2011 off the Pacific coast of Tohoku Earthquake and landslides in  
453 Shirakawa city, Fukushima. Report on the debriefing session of landslide hazards triggered by the 2011 off the Pacific  
454 coast of Tohoku Earthquake, Japan Landslide Society.
- 455 Tika, T.E., Vaughan, P.R., Lemos L., 1996. Fast shearing of pre-existing shear zone in soil. *Géotechnique* 46, 197-233.
- 456 Tiwari, B., Marui, H., 2004. Objective oriented multistage ring shear test for shear strength of landslide soil. *Journal of*  
457 *Geotechnical and Geoenvironmental Engineering* 130, 217-222.
- 458 Tobita, T., Iai, S., Iwata, T., 2010. Numerical analysis of near-field asymmetric vertical motion. *Bulletin of the Seismological*  
459 *Society of America* 100, 1456-1469
- 460 Unno, T., Kazama, M., Uzuoka, R., Sento, N., 2006. Change of moisture and suction properties of volcanic sand induced by  
461 shaking disturbance. *Soils and Foundations* 46, 519-528.
- 462 Unno, T., Kazama, M., Sento, N., Uzuoka, R., 2008. Liquefaction of unsaturated sand considering the pore air pressure and  
463 volume compressibility of the soil particle skeleton. *Soils and Foundations* 48, 87-99.
- 464 Voight, B., Janda, R.J., Glicken, H., Douglass P.M., 1983. Nature and mechanisms of the Mount St. Helens rock-slide  
465 avalanche of 18 May 1980. *Géotechnique* 33, 243-273.
- 466 Wang, G., 2000. An experimental study on the mechanism of fluidized landslide — with particular reference to the effect of  
467 grain size and fine-particle content on the fluidization behavior of sands. PhD thesis, Kyoto University. 209 pp.
- 468 Wang, G., Sassa, K., Fukuoka, H., Tada T., 2007. Experimental study on the shearing behavior of saturated silty soils based  
469 on ring shear tests. *Journal of Geotechnical and Geoenvironmental Engineering ASCE* 133, 319-333.
- 470 Wang, G., Suemine, A., Schulz, W.H., 2010. Shear-rate-dependent control on the dynamics of rainfall-triggered landslides,  
471 Tokushima Prefecture, Japan. *Earth Surface Processes and Landforms* 35(4), 407-416.
- 472 Wesley, L.D., 1973. Some basic engineering properties of halloysite and allophane clays in Java, Indonesia. *Géotechnique*  
473 23, 471-494.
- 474 Wesley, L.D., 1977. Shear strength properties of halloysite and allophane clays in Java, Indonesia. *Géotechnique* 27,  
475 125-136.
- 476 Yang, J., 2007. On seismic landslide hazard assessment. *Géotechnique* 57, 707-713.
- 477 Yang, J., Sato, T., 2000. Interpretation of seismic vertical amplification observed at an array site. *Bulletin of the*  
478 *Seismological Society of America* 90, 275-285.

Captions:

**Fig. 1.** Locations of the epicenter of the 2011 Tohoku earthquake off the Pacific coast of Japan and the landslides presented in this study (after Google Map). ○: Location of city; ●: Location of landslide.

**Fig. 2.** Geological map of the study area (after Geological Survey of Japan, 2003)

**Fig. 3.** Topographic maps. (a) Hanokidaira landslide area (based on the planning map of Shirakawa City with a contour interval of 2 m); (b) and (c): Shirasawa and Oshino areas, respectively (based on the digital map of Geospatial Information Authority of Japan with a contour interval of 10 m).

**Fig. 4.** Hanokidaira landslide. (a) Oblique view (after Takeshi 2011); (b) view of the left side margin and sliding surface; (c) buried grass on the golf driving range and palaeosol layer above the grass; (d) muddy striae on the left-side margin; (e) splashed mud on left-side margin; (f) longitudinal section along line I-I'; (g) outcropped palaeo-valley in the source area of the Hanokidaira landslide. PV-M: main palaeo-valley; PV-T: tributary of the main palaeo-valley. S1 and S1': Sampling locations for disturbed and intact samples of palaeosol, respectively.

**Fig. 5.** Shirasawa landslide. (a) Oblique view (after Takeshi 2011); (b) sliding surface and outcropping palaeosol on the source area; (c) Muddy striae and splashed mud on the left side margin.

**Fig. 6.** Oshino landslide. (a) Oblique view, (b) Outcropped sliding surface and palaeosol; (c) muddy striae and splashed mud on left side of the margin; (d) longitudinal section along I-I'.

**Fig. 7.** Seismic records and maximum acceleration from the K-NET Shirakawa station (a-c), the JMA Shirakawa-shi Kakunai station (d-f), and the estimated seismic waves in the Hanokidaira area (g-i). EW, NS, UD: seismic motion in the direction of east–west, north–south, and up–down (vertical).

**Fig. 8.** Drained shear strength and failure envelopes of the intact and remolded sample S1 at natural moisture content by direct shear box tests. Also showing the failure envelopes of the intact and remolded sample S2 at saturated state obtained by triaxial compression tests.

**Fig. 9.** Undrained cyclic shear tests on saturated samples S1 (a) and S2 (b). The dry densities (after consolidation) were  $0.70$  and  $0.51 \text{ g cm}^{-3}$  for S1 and S2, respectively.

**Fig. 10.** Undrained shear test on sample S2 (moisture content: 140%). (a) Time series data of stresses, pressure and shear displacement; (b) vertical displacement (positive indicates sample consolidation). The dry density of the sample after consolidation was  $0.55 \text{ g cm}^{-3}$ .

**Fig. 11.** Residual shear resistance of saturated S1 at different shear rates.

## Figures

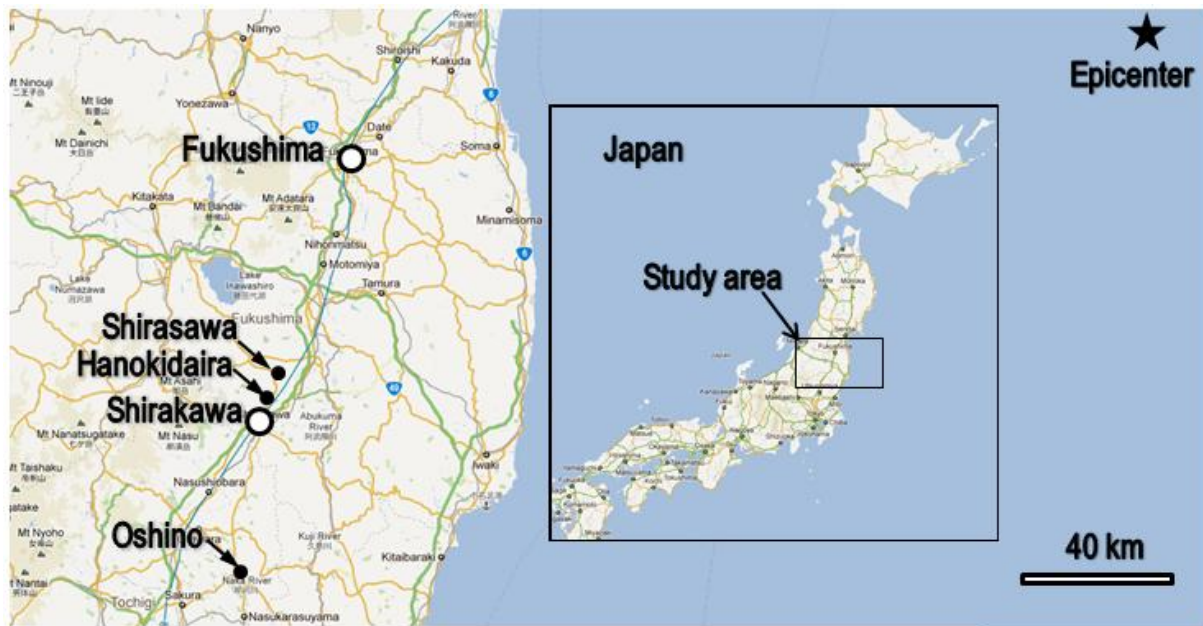


Fig. 1

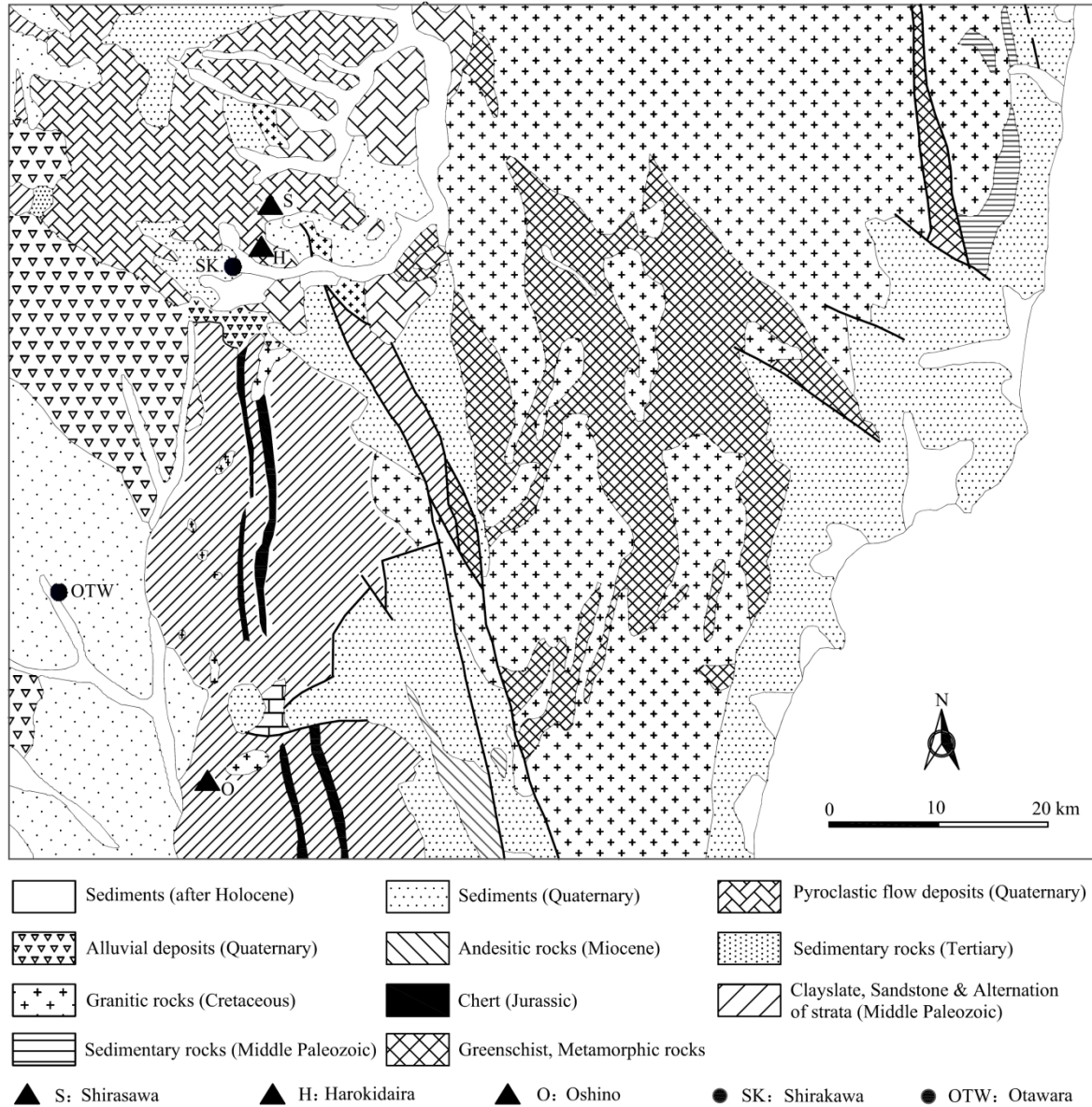


Fig. 2 Geological map of study area



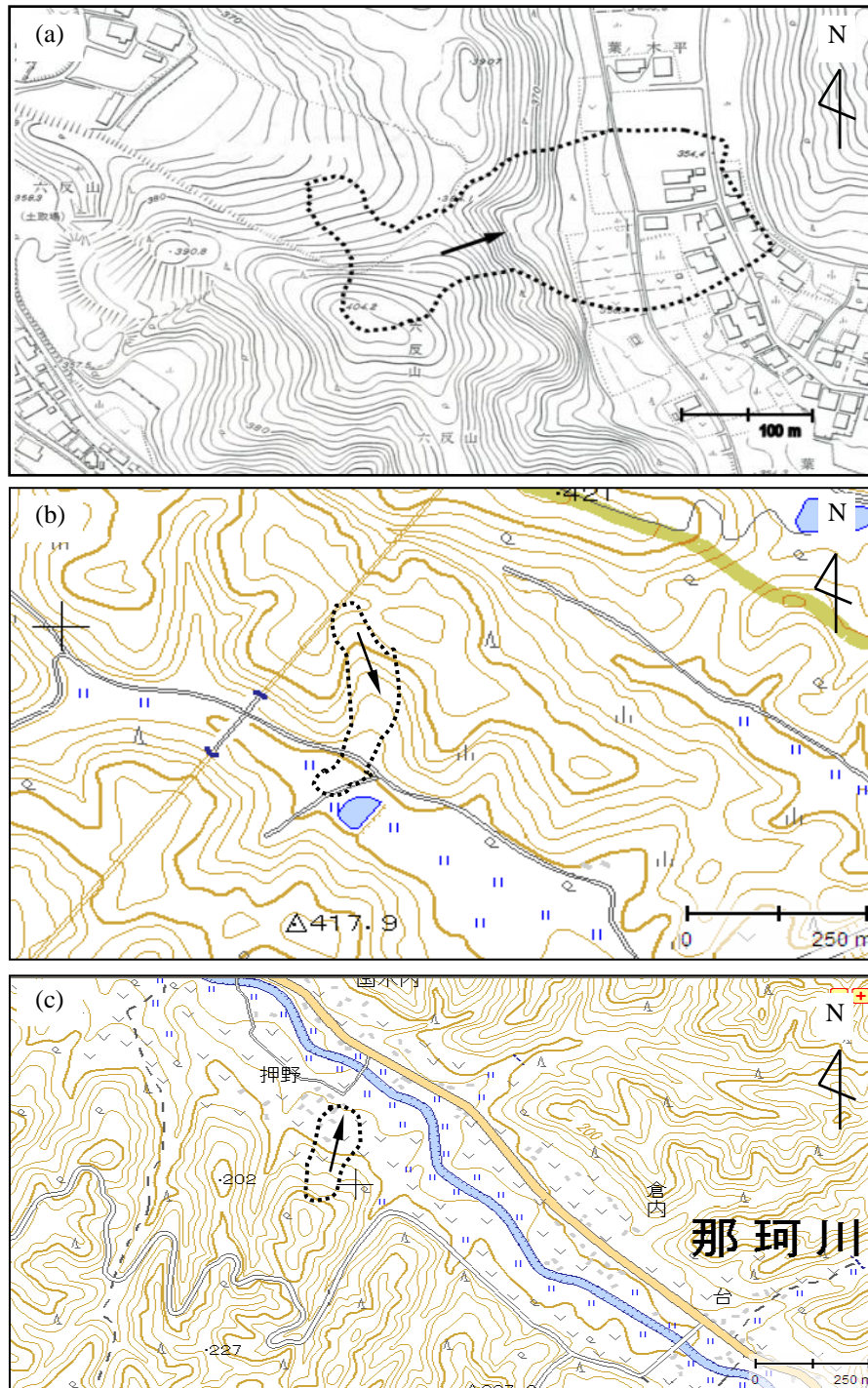


Fig. 3.

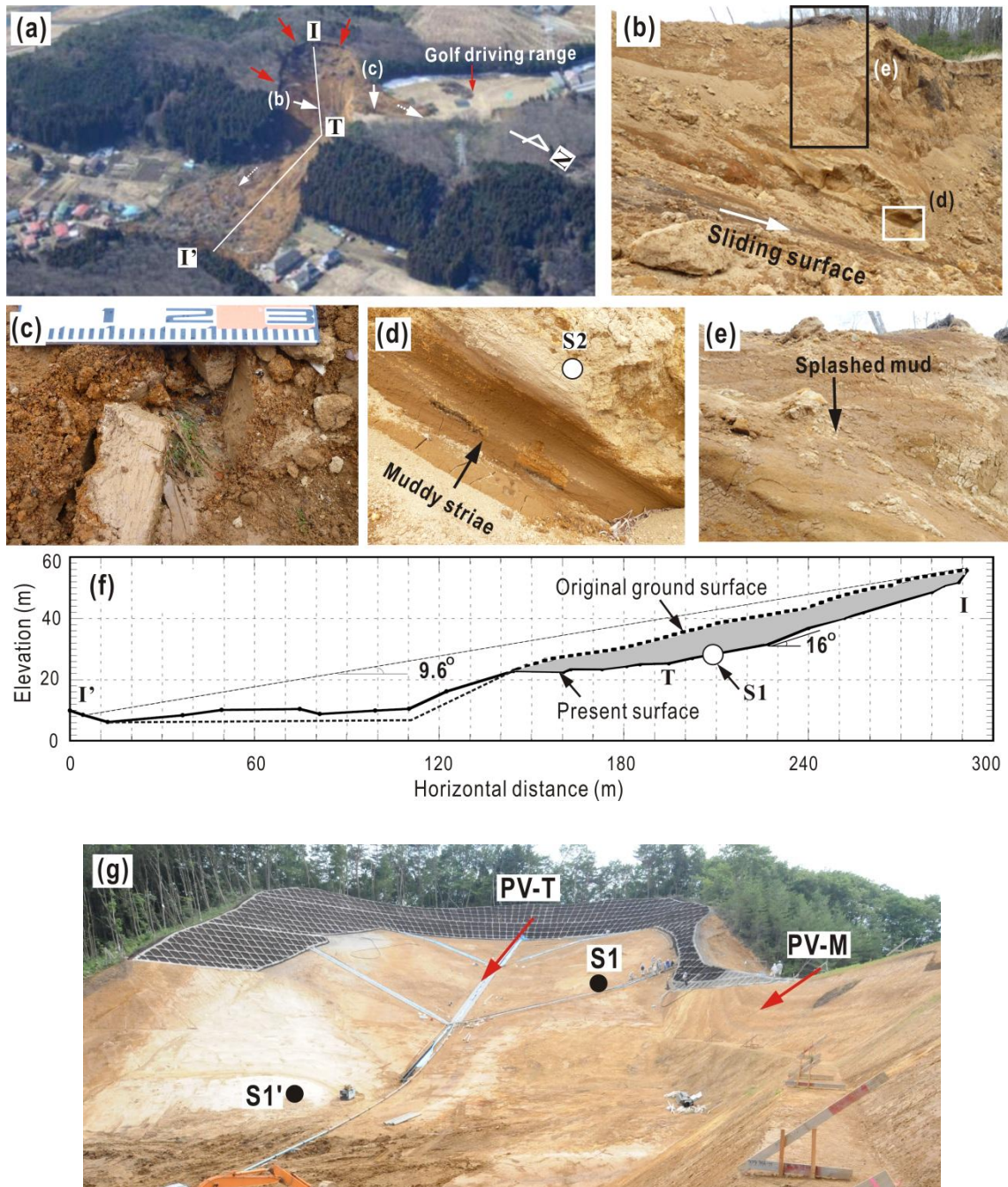


Fig. 4.



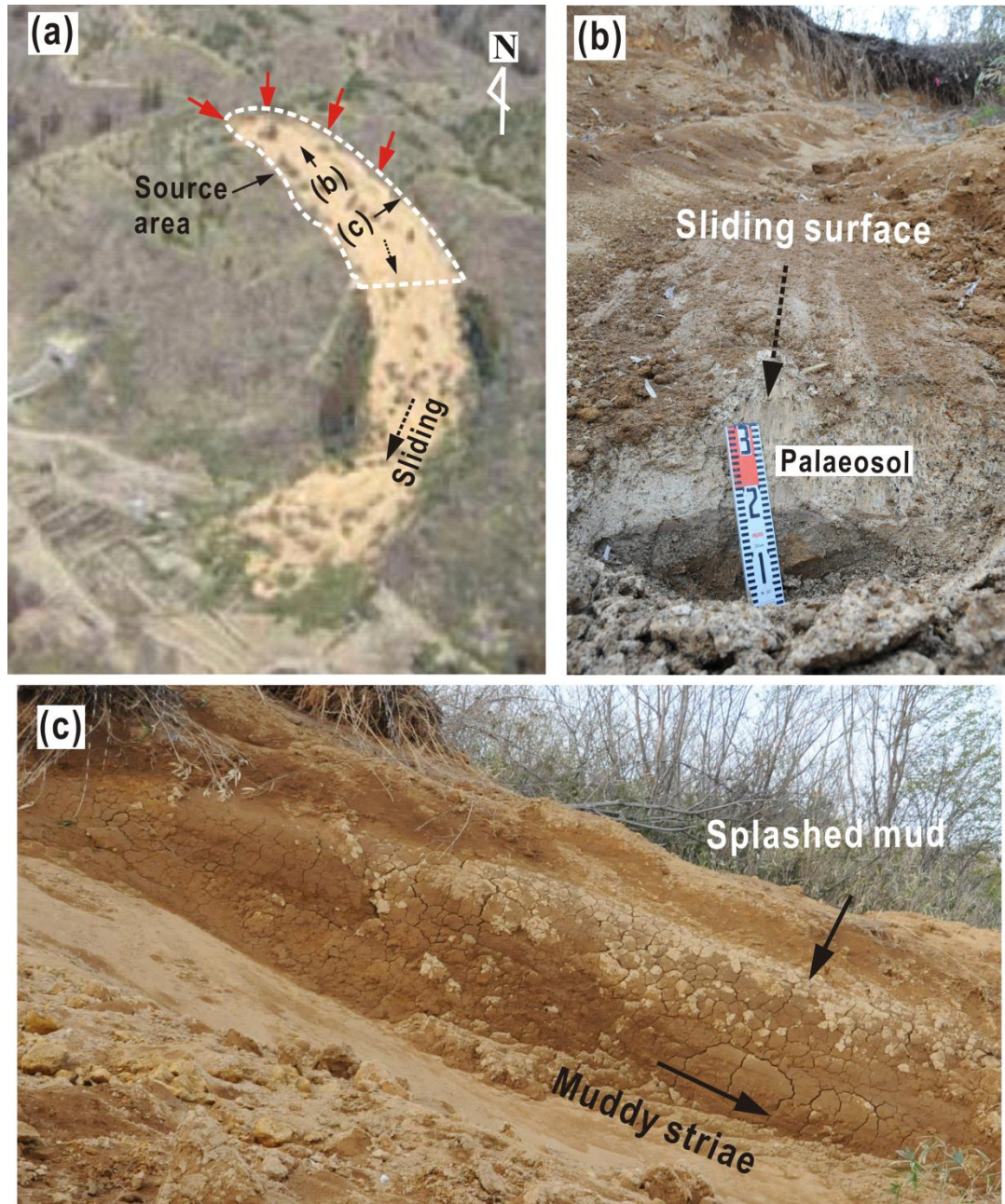


Fig. 5.

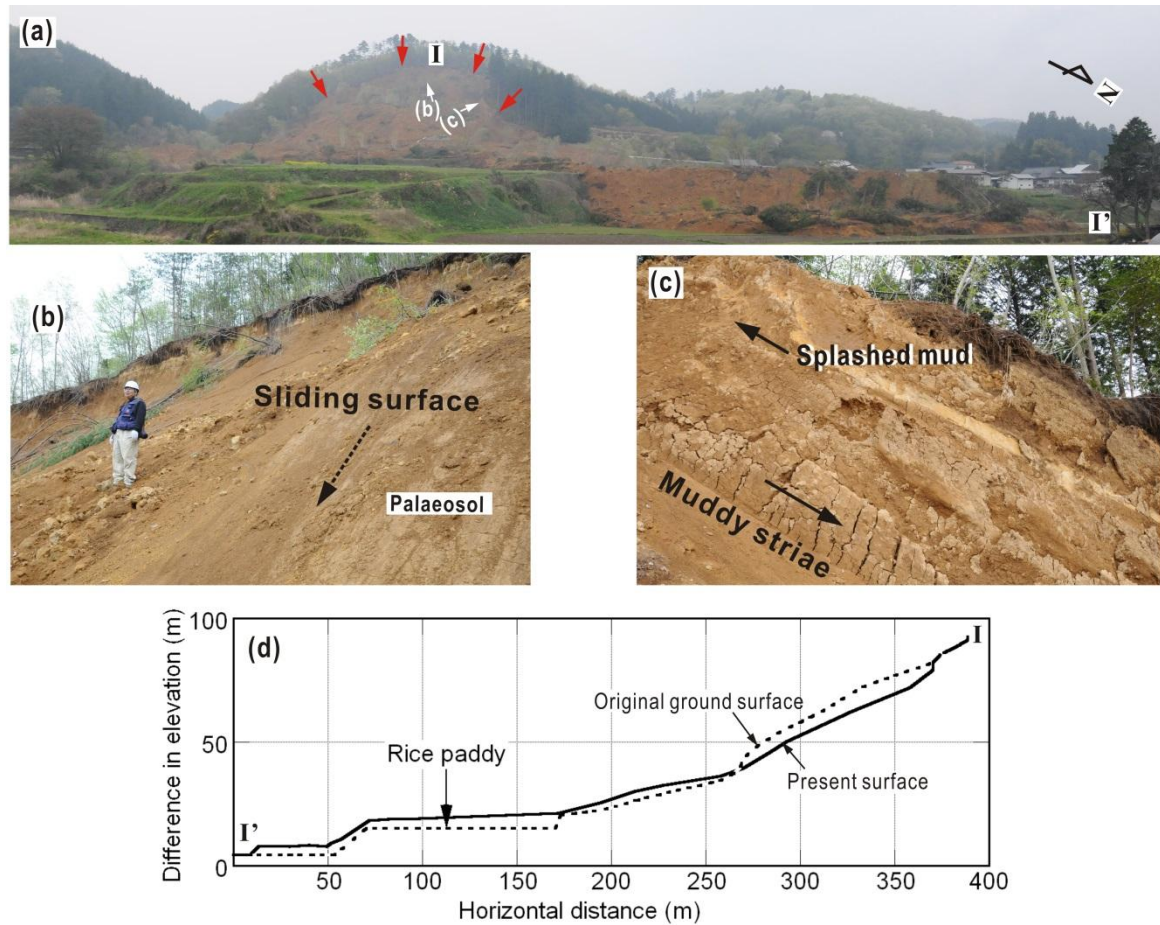


Fig. 6.



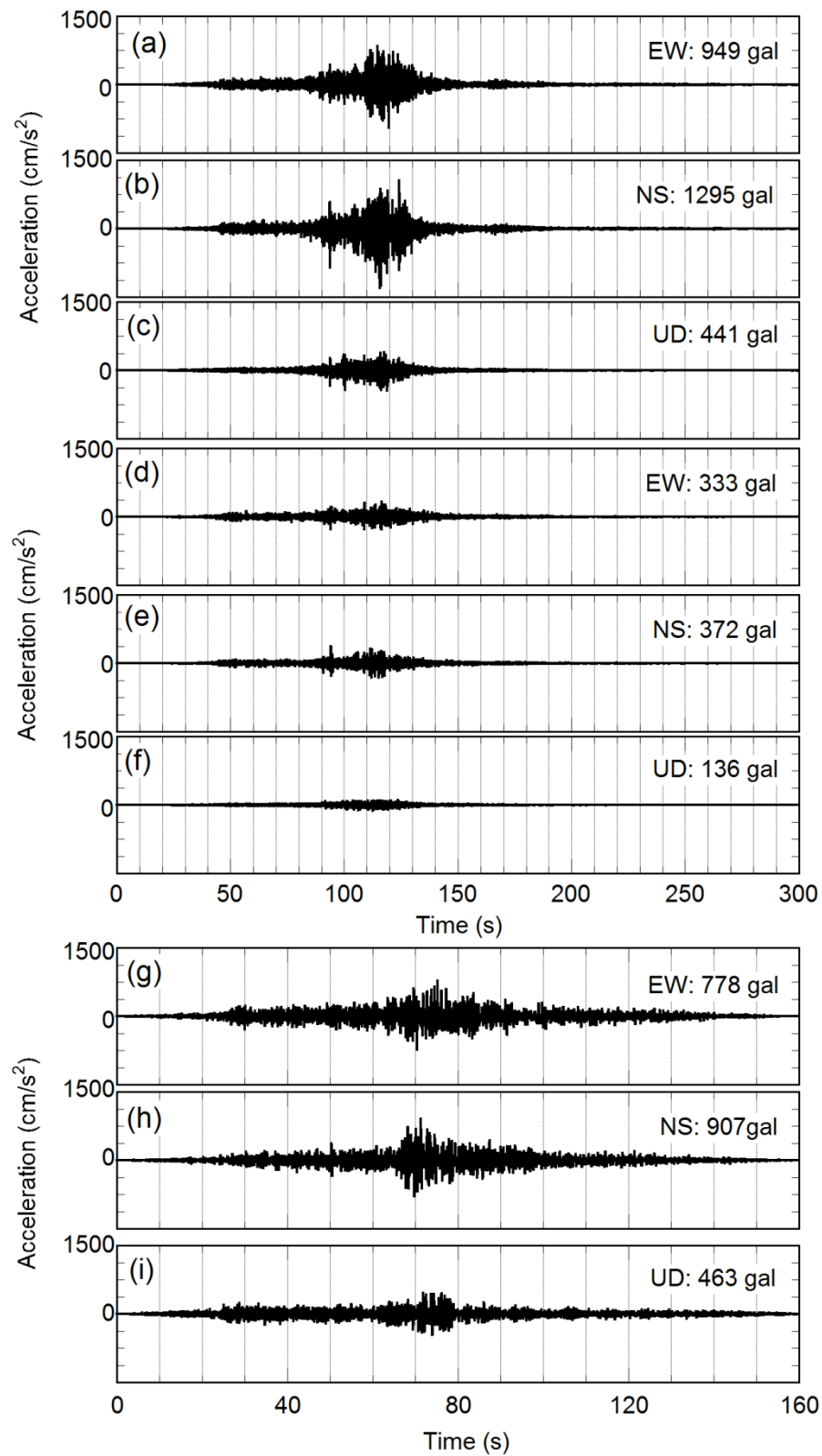


Fig. 7.

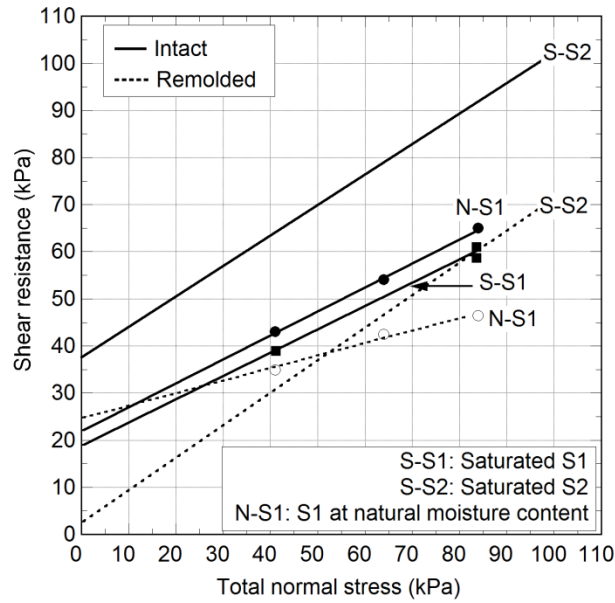


Fig. 8

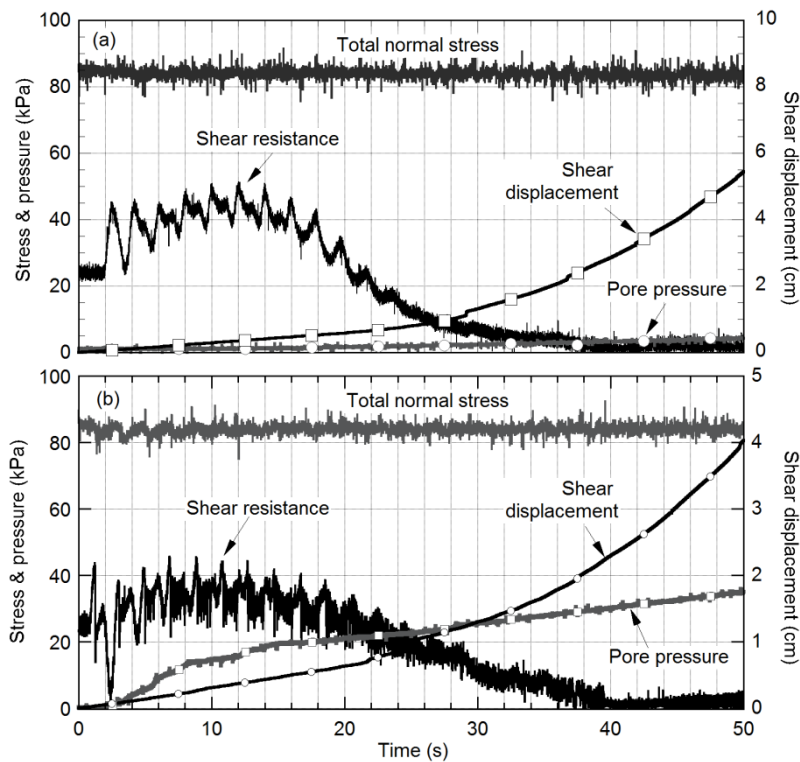


Fig. 9.

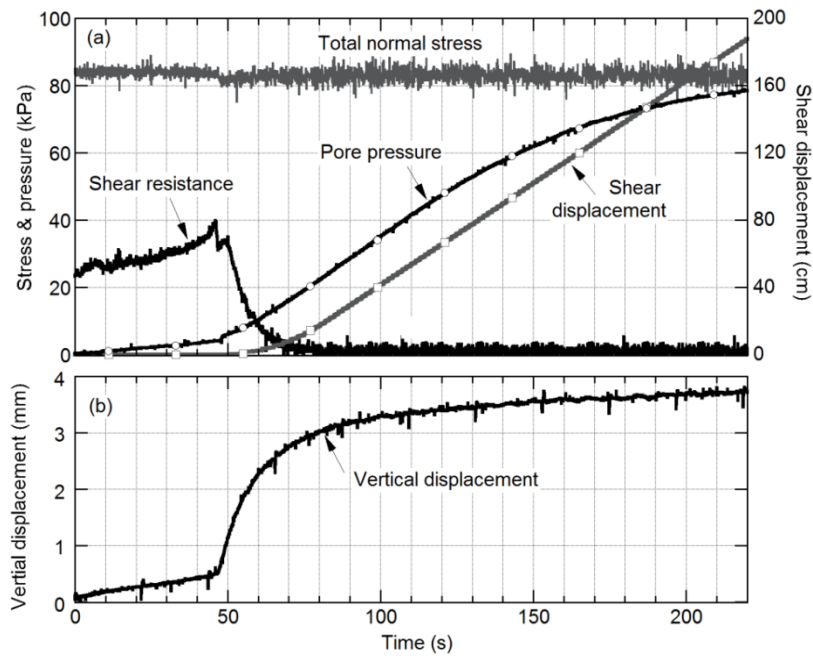


Fig. 10

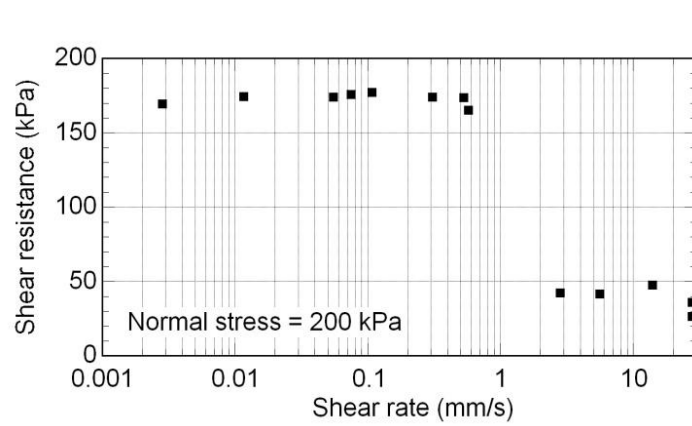


Fig. 11